PHYSICAL REVIEW D **77,** 025007 (2008)

Signatures of the transition from galactic to extragalactic cosmic rays

Roberto Aloisio and Veniamin Berezinsky
INFN, Laboratori Nazionali del Gran Sasso, I-67010 Assergi (AQ), Italy

Pasquale Blasi
INAF, Osservatorio Astrofisico di Arcetri, Largo E. Fermi, I–50125 Firenze, Italy
and INFN, Laboratori Nazionali del Gran Sasso, I-67010 Assergi (AQ), Italy

Sergey Ostapchenko
Institut für Experimentelle Kernphysik, University of Karlsruhe, 76131 Karlsruhe, Germany
and D. V. Skobeltsyn Institute of Nuclear Physics, Moscow State University, 119992 Moscow, Russia
(Received 7 August 2007; published 9 January 2008)

We discuss the signatures of the transition from galactic to extragalactic cosmic rays in different scenarios, giving the most attention to the dip scenario. The dip is a feature in the diffuse spectrum of ultrahigh-energy protons in the energy range 1×10^{18}–4×10^{19} eV, which is caused by electron-positron pair production on the cosmic microwave background radiation. The dip scenario provides a simple physical description of the transition from galactic to extragalactic cosmic rays. Here we summarize the signatures of the pair-production dip model for the transition, most notably the spectrum, the anisotropy, and the chemical composition. The main focus of our work is, however, on the description of the features that arise in the elongation rate and in the distribution of the depths of shower maximum $X_{\max}$ in the dip scenario. We find that the curve for $X_{\max}(E)$ shows a sharp increase with energy, which reflects a sharp transition from an iron-dominated flux at low energies to a proton-dominated flux at $E \sim 10^{18}$ eV. We also discuss in detail the shape of the $X_{\max}$ distributions for cosmic rays of given energy and demonstrate that this represents a powerful tool to discriminate between the dip scenario and other possible models of the transition.

DOI: 10.1103/PhysRevD.77.025007 PACS numbers: 12.60.Jv, 95.35.+d, 98.35.Gi

I. INTRODUCTION

The observed spectrum of cosmic rays (CR) has a power-law shape at energies between $E \sim 10^{10}$ eV and $E \sim 10^{15}$ eV, while several features are observed at higher energies. The *knee* in the all-particle spectrum consists of a steepening of the power-law behavior from $E^{-2.7}$ to $E^{-3.1}$. This feature coincides with the knee in the proton spectrum, but the latter is more pronounced than the knee in the all-particle spectrum and might be related to a cutoff in the proton spectrum associated with the maximum energy of accelerated protons at the sources. The knees in the spectra of heavier nuclei are found at larger energies but they are not measured as yet with the same level of accuracy. These knees do not reveal themselves as any particular feature in the all-particle spectrum.

At energies $E_{2\mathrm{kn}} \approx (4\text{–}8) \times 10^{17}$ eV a weak spectral steepening is observed by the Akeno, Yakutsk, Fly's Eye, and HiRes detectors. This faint feature is referred to as the *second knee*. At energy $E_a \approx 1 \times 10^{19}$ eV a very pronounced flattening of the spectrum, called the *ankle*, appears. This feature was first discovered by the Haverah Park detector at the end of the 1970s. It is now seen by most experiments, although the energy where the ankle is observed depends on the method of analysis adopted for the spectral reconstruction and is affected by systematic errors in the energy determination.

Extrapolating the spectrum from higher to lower energies, one finds the beginning of the ankle at energy $E_a \sim 1 \times 10^{19}$ eV. The HiRes Collaboration defined the ankle as the intersection of two power-law spectra, just below and just above E_a. The intersection energy found in this way is $E' \approx 5 \times 10^{18}$ eV (for a review see [1]).

The region between the proton knee and the ankle is naturally to be considered as the region where the galactic cosmic ray spectrum ends and the extragalactic component begins. However, the description of this transition is very model dependent, and high quality observational data are needed in order to discriminate among different models.

A. Standard model of galactic cosmic rays

The standard model for the origin of cosmic rays in the lower energy part of this transition region is based on the *supernova paradigm*: young supernova remnants (SNRs) may provide the observed energy density $\omega_{\mathrm{cr}} \sim 1 \times 10^{-12}$ erg/cm^3 of the galactic cosmic rays and accelerate particles up to a maximum energy $E_{\max} \sim (1\text{–}3) \times 10^{15}$ eV for protons (higher by a factor Z for nuclei with charge Z) [2]. Particle acceleration takes place through first order Fermi acceleration at the supernova shock. The highest energies mentioned above are reachable only if the magnetic field in the shock proximity is amplified by a factor 100–1000 with respect to the interstellar field, and is rearranged topologically in order to lead to particle scat-

tering at approximately the Bohm limit [3]. Magnetic field amplification roughly to this level has been observed in x rays [4] and can be explained in terms of streaming instability induced by cosmic rays [5], although alternative models of instability cannot be excluded at the present time. The process of particle acceleration in the presence of dynamical reaction of the accelerated particles and magnetic field amplification has been studied recently in [3,6,7]. Phenomenological descriptions of the acceleration process and interesting consequences have recently been investigated in [8], among other papers. A model of the effects of acceleration in SNRs on the overall spectrum of cosmic rays observed at the Earth has been presented in [9].

The amplification of the magnetic field takes place in a complex chain of nonlinear effects: particle acceleration becomes efficient when the field is amplified, but streaming instability occurs fast enough when particles are accelerated effectively [5]. This situation evolves into a self-regulating nonlinear system.

As discussed in [10], the maximum energy achieved by particles grows with time during the free expansion phase, but saturates at the beginning of the Sedov phase: particles injected at the beginning of the free expansion phase or at the beginning of the Sedov phase basically reach the same maximum energy, thereby confirming that the most important stage for particle acceleration in SNRs is the initial part of the Sedov phase. During the Sedov phase the shell slows down, and the maximum energy at a given age t of the remnant decreases as a consequence of the lack of confinement in the shock region of particles accelerated to larger energies at previous times. Moreover, the effectiveness of magnetic field amplification decreases. This situation leads to an interesting situation: particles with energy in a narrow range around $E_{\rm max}(t)$ escape from the upstream region, with a spectrum that, at a given time, is roughly a delta function around $E_{\rm max}(t)$. The position of the delta function decreases in energy while time progresses. At the same time, lower energy particles keep being accelerated and stay within the shock. These particles will escape the SNR only at much later times. The flux of cosmic rays injected by SNRs is the superposition of the flux of particles escaping from upstream, integrated over time, and the flux of particles accumulated behind the SNR shock and summed over all supernova events. In the classical theory of particle acceleration the former contribution is unimportant because the spectrum of accelerated particles is always steeper than E^{-2} and the total energy carried by particles with $E \sim E_{\rm max}(t)$ is negligible. In modern nonlinear theories of particle acceleration at shocks, this is not the case: the spectra in the highest energy region are flatter than E^{-2}, and particles with $E \sim E_{\rm max}(t)$ carry away from the shock an appreciable amount of energy (e.g. the shock becomes radiative). In Ref. [8] the authors show that the integration over time of the flux of particles escaping from upstream during the Sedov phase sums up to a power law with slope $\sim$2. In [9] the contribution of the particles confined in the shock region is calculated in the context of nonlinear theory.

The spectra of different nuclei calculated in [2,9] agree well with observations of ATIC, JACEE, and KASCADE, with the maximum energy being rigidity dependent, $E_{\rm max} \approx 2Z \times 10^{15}$ eV, where Z is the charge of the nucleus. The rigidity-dependent character of $E_{\rm max}$ is the basic feature of this model. At $E \gtrsim E_{\rm max}$ the spectra of all nuclei are predicted to have a sharp cutoff.

Clearly, these predictions can be compared with observations only after dressing the *standard model* with suitable prescriptions about the diffusion of cosmic rays in the interstellar medium. With the standard prescription of the diffusion coefficient $D(E) \propto E^{0.3-0.6}$, the standard model cannot easily explain the excess of helium flux below the knee [11] and the low level of anisotropy observed at the knee [12,13]. We should, however, keep in mind that the acceleration of helium and other elements in all existing calculations is carried out in a very phenomenological way, and that the expectations concerning diffusion are not confirmed in a straightforward way by more accurate calculations of cosmic ray propagation in the Galaxy [14].

Based on the observation of the proton knee $E^{p}_{\rm kn} \approx (2\text{–}3) \times 10^{15}$ eV, the end of the galactic cosmic ray spectrum in the context of the ''standard model'' is predicted to coincide with the iron knee, $E^{\rm Fe}_{\rm kn} \approx (5\text{–}8) \times 10^{16}$ eV. This is the fundamental conclusion of the standard model. If the transition from galactic to extragalactic CRs occurs at the ankle, $E_a \sim 1 \times 10^{19}$ eV, the standard model must be supplemented by additional acceleration mechanisms able to boost the maximum energy of the accelerated particles well above $E^{\rm Fe}_{\rm kn}$. In [9] reacceleration is discussed as a possible mechanism. Since the highest energy particles are involved in this process, the chemical composition at 1×10^{17}–1×10^{19} eV must be dominated by iron nuclei.

B. Extragalactic cosmic rays

We move now to examining the extragalactic component of cosmic rays. The traditional model for the transition from galactic to extragalactic CRs is the *ankle model* [15]. The attractiveness of this model is provided by its natural character: the flat extragalactic spectrum crosses the steep galactic spectrum, and the ankle appears at an energy just above the intersection of the two components. Another attractive feature of the model is connected with the generation spectrum of the extragalactic component which can be as flat as $E^{-\gamma_g}$ with $\gamma_g \sim 2$. This slope is close to that predicted by Fermi acceleration at nonrelativistic shocks ($\gamma = 2$–2.5) and at ultrarelativistic shocks ($\gamma_g = 2.2$–2.3). It is, however, important to keep in mind that these predicted slopes are rather strongly model dependent in that the spectra can be either flatter, because of the dynamical reaction of accelerated particles, or steeper, for instance,

because of the compression of the magnetic field at the shock surface [16].

The observed dip at $1 \times 10^{18} \leq E \leq 4 \times 10^{19}$ eV can be explained in the context of the ankle model following the idea put forward by Hill and Schramm in 1985 [17] in the framework of a two-component model: a steep galactic component encounters a flat extragalactic component and produces the dip structure. This idea was later used in the calculations of Ref. [18].

The drawback of the ankle model resides in its incompatibility with the standard model illustrated above. Indeed, if iron nuclei start to disappear at some energy above the iron knee $E_{\rm kn}^{\rm Fe} \approx (5\text{–}8) \times 10^{16}$ eV, which particles should fill the gap between the iron knee and the ankle?

The pair-production dip model provides an alternative interpretation of the transition. As has been originally proposed in [19], the dip can be produced by extragalactic protons with a power-law spectrum due to e^+e^- pair production on cosmic microwave background (CMB) photons. This feature has been studied recently in [20–22]. It is reliably observed in experimental data (see Fig. 1), provided that the generation spectrum is $\propto E^{-\gamma_g}$ with $\gamma_g \approx 2.6\text{–}2.7$. It is important to stress that this slope refers to the *average*, effective spectrum of the sources contained in a shell between redshifts z and $z + dz$. It can be obtained either by assuming that all sources contribute the same spectrum $E^{-2.7}$ with a cutoff at the same maximum energy, or by assuming that single sources contribute a flatter spectrum (say $E^{-2.3}$) with maximum energies which depend on the source luminosity and other intrinsic properties [22,23].

At energies below $E_{\rm cr} \approx 1 \times 10^{18}$ eV the calculated extragalactic spectrum of protons becomes flat, especially in the case of diffusive propagation (see Sec. II), while the galactic spectrum is very steep ($\propto E^{-3.1}$). Therefore somewhere below $E_{\rm cr}$ the extragalactic spectrum must intersect the steeper ($\propto E^{-3.1}$) galactic spectrum. The transition occurs at the second knee. The prediction of this model—the strong dominance of the proton component at $E > E_{\rm cr}$—is confirmed by HiRes, HiRes-Mia, and Yakutsk data, while Akeno and Fly's data favor a mixed composition. The dip-based transition model agrees perfectly with the galactic standard model. It is important to notice that the basic ingredient of a transition, the intersection of a steep galactic spectrum with a flatter extragalactic one, remains the same in both the dip and the ankle scenarios.

An alternative to both the dip scenario and the ankle scenario has been put forward in [24,25], in which the

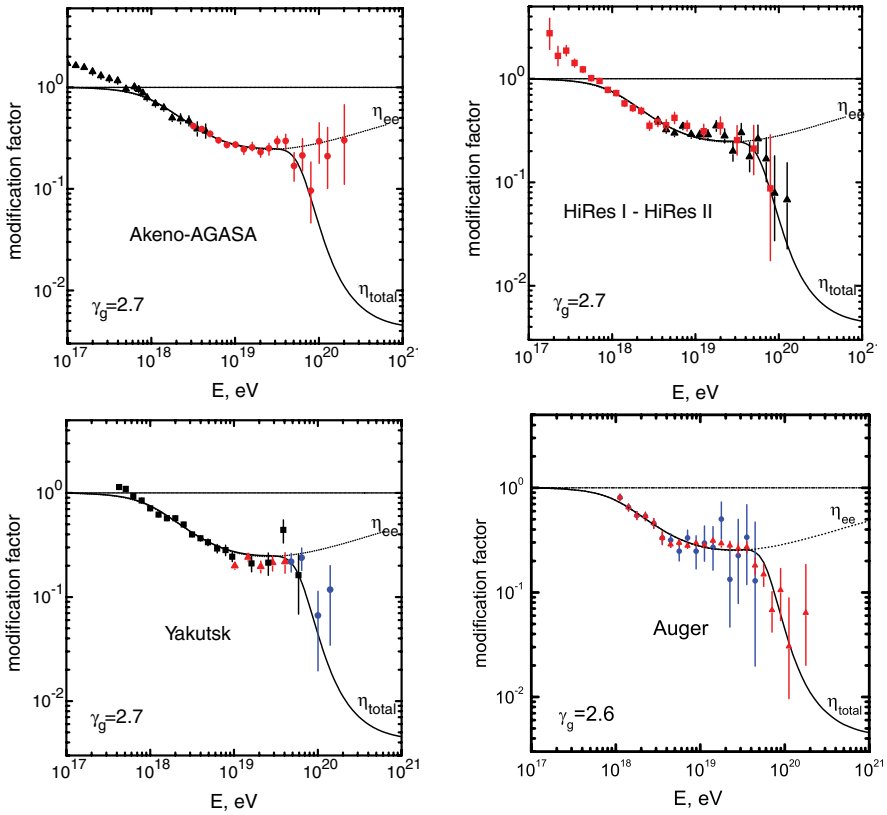

FIG. 1 (color online). Predicted dip in comparison with the AGASA [48], HiRes [49], Yakutsk [50], and Auger [51] data. The latter are presented as hybrid data, shown by circles, and combined data (surface detector data above 4.5 EeV and fluorescence data below), shown by triangles. The comparison of the dip with Auger data is taken from Ref. [29].

chemical composition of the injected extragalactic cosmic rays has been assumed to be complex, with a mixture of elements from hydrogen to iron. The photodisintegration of nuclei interacting with IR and CMB radiations leads to a spectrum at $E \geq 3 \times 10^{18}$ eV that can fit the observed all-particle spectrum if an injection spectrum is as flat as $E^{-\gamma_g}$ with $\gamma_g = 2.1$–2.3. A review of the mixed-composition model has recently been presented in [26].

C. Experimental signatures of the galactic-extragalactic transition

There are basically three types of data which may provide a clue to the model for the transition from galactic to extragalactic cosmic rays. They are *spectra, anisotropy*, and *chemical/mass composition*.

The *energy spectrum* is the most important source of information on the transition region, since it is measured with the best accuracy in comparison with the other two physical quantities. In general, a transition from a steep to a flat spectrum is accompanied by a flattening of the all-particle spectrum. This is certainly true in the case of the ankle, but it does not need to be so in the most general case. A typical example is provided by the transition from lighter to heavier elements around the knee: one might expect a flattening at each transition, but none is observed in the all-particle KASCADE spectrum. In the case of the dip scenario, the transition occurs due to the intersection of a steep galactic spectrum $\propto E^{-3.1}$ with a flat extragalactic spectrum below 1×10^{18} eV. But because of the fact that the transition occurs in a narrow energy range, it leaves a very weak spectral feature in the all-particle spectrum, known as the second knee. The flatness of the extragalactic spectrum in the dip model is a general prediction, valid in both cases of straight line and diffusive propagation.

The pair-production dip at $1 \times 10^{18} \leq E \leq 4 \times 10^{19}$ eV is a remarkable spectral feature which characterizes the transition. It has a very peculiar shape, and its measurement with high precision may be considered as an evidence of the fact that the particles detected in this energy region are extragalactic protons (with at most a small contamination of heavier elements) propagating through CMB. It is very important that the particle energies measured in different experiments operating in this energy region could be calibrated by the position of the dip. After this calibration the fluxes measured in different experiments agree with high precision, and this suggests that the dip is not just an accidental feature in the spectrum. This agreement of the dip with the data gives the main support of the *dip-based model of the transition*.

The third model of transition, which is now the subject of discussion, is the *mixed-composition model*. Like the ankle model, it explains the observed dip in the framework of the Hill-Schramm two-component model [17]. The low-energy part of the dip is given by the galactic component and the high-energy part by the extragalactic component of cosmic rays. The transition occurs at $E \sim 3 \times 10^{18}$ eV, and thus the model agrees well with the standard model. The injection spectrum required at the sources is compatible with the one typically expected from diffusive shock acceleration in its basic version. The mixed-composition model is based on the assumption that the chemical composition of cosmic rays in extragalactic sources is similar to that which can be inferred for SNRs after correcting for spallation during propagation. It is, however, easy to imagine several astrophysical situations in which this does not need to be the case. Both the ankle model and the mixed-composition model are left with the tough problem of justifying the accidental coincidence of the observed dip location with the dip generated by pair production, which can be predicted with high accuracy.

Anisotropy may, in principle, provide information on the transition: at the transition energy, the anisotropy is expected to shift from that induced by the location of the sun in the galactic disc to the more isotropic extragalactic cosmic ray flux. A small anisotropy may be expected in the case of diffusive propagation in the low-energy regime (10^{17}–10^{18} eV), as associated with the nearest source. The expected anisotropy is, however, likely to be undetectable. The anisotropy connected with the galactic sources can be detected in the end of the galactic spectrum (see the discussion in [27]). This possibility is realistic for the ankle transition, when the maximum energy of the accelerated particles by some additional acceleration mechanism may allow particles to reach 1×10^{19} eV, and the galactic spectrum cutoff is caused by insufficient confinement by the galactic magnetic field. In this case the galactic protons from a source can reach the observer, undergoing a small deflection angle.

The *chemical composition* gives the most stringent constraint on the transition models. In the ankle model cosmic rays are expected to be galactic and iron dominated up to energies in excess of 10^{19} eV. In the mixed-composition model the transition from galactic to extragalactic cosmic rays is completed at energies around 3×10^{18} eV, and the chemical composition in this energy region is mixed. In the dip scenario, the transition is completed at energy $\sim 1 \times 10^{18}$ eV, and the composition at this energy is already proton dominated.

In this paper we concentrate on the signatures of the dip scenario in terms of the elongation rate and a distribution of shower maximum at given energy of the primary cosmic rays. We demonstrate that the elongation rate, irrespectively of the absolute normalization of $X_{\max}(E)$, which is more model dependent, has, in the dip model, a *sharp transition* from a composition dominated by iron nuclei to a proton-dominated composition. This sharp transition is absent in the two other models, ankle and mixed composition, and it may be considered as a specific signature of the dip model.

We also calculate the $X_{\max}$ distribution for different energies of the primaries and propose that the distribution of shower maximum may be an effective tool to discriminate between the mixed-composition model and the dip scenario.

The paper is organized as follows: in Sec. II we summarize the main predictions of the dip model in terms of the CR spectrum and the expected anisotropy. In Sec. III we discuss the ankle and the dip scenarios in terms of the predicted mean elongation rate. The effect on the distribution of $X_{\max}$ is discussed in Sec. IV. We conclude in Sec. V.

II. THE DIP MODEL: SIGNATURES IN THE SPECTRUM AND ANISOTROPY

We start with a short description of the dip-based model of the transition.

The pair-produced dip is a faint feature in the spectrum of extragalactic ultrahigh-energy (UHE) protons propagating through the CMB. Being a quite faint feature, the dip is not seen well when the spectrum is plotted in its basic form, $\log J(E)$ vs $\log E$. The dip appears more pronounced when it is shown in terms of the *modification factor*, as introduced in [19,28]. The modification factor is defined as the ratio of the diffuse spectrum $J_p(E)$, calculated with all energy losses taken into account, and the unmodified spectrum $J_p^{\rm unm}$, where only adiabatic energy losses (red shift) are included: $\eta(E) = J_p(E)/J_p^{\rm unm}(E)$. The spectrum $J_p(E)$ can be calculated from the conservation of the number density of particles as

$$n_p(E, t_0)dE = \int_{t_{\min}}^{t_0} dt Q_{\rm gen}(E_g, t)dE_g, \qquad (1)$$

where $n_p(E, t_0)$ is the space density of UHE protons at the present time, t_0, $Q_{\rm gen}(E_g, t)$ is the generation rate per comoving volume at cosmological time t, and $E_g(E, t)$ is the generation energy at time t for a proton with energy E at $t = t_0$. This energy is found from the loss equation $dE/dt = -b(E, t)$, where $b(E, t)$ is the rate of energy losses at epoch t. The spectrum, Eq. (1), calculated for a power-law generation spectrum $\propto E^{-\gamma_g}$ and for a homogeneous distribution of sources, is called the *universal spectrum* [20].

Since the injection spectrum $E^{-\gamma_g}$ enters both the numerator and the denominator of $\eta(E)$, one may expect that the modification factor depends weakly on γ_g.

In Fig. 1 we show the comparison of the modification factor calculated for $\gamma_g = 2.7$ with the observational data of AGASA, HiRes, and Yakutsk, and for Auger data, where $\gamma_g = 2.6$ was used. The presence of the dip in the modification factor $\eta_{ee}(E)$ is confirmed by the data at energies below $E \approx 4 \times 10^{19}$ eV. Above this energy the photopion production dominates (see Fig. 1). Fly's Eye data, not shown here, confirm the dip equally well. The Auger spectrum is also in agreement with the dip scenario for $\gamma_g = 2.6$, though with a worse χ^2.

The dip presented in Fig. 1 is calculated in terms of the universal spectrum, i.e. for a homogeneous distribution of the sources and assuming no source evolution. In this case we need only two free parameters for the comparison of the dip with observational data: γ_g and an overall normalization constant (or energy production rate per unit time and volume—emissivity $\mathcal{L}$). For 18–22 energy bins in each experiment, the agreement is characterized by $\chi^2/\text{d.o.f.} \approx 1$. In the case of the Auger data $\chi^2/\text{d.o.f.}$ is larger [29].

Despite this impressive agreement with most experimental data, one has to assess the effect of numerous physical effects that may spoil the agreement. As was demonstrated in Refs. [20,22], the inclusion of the discreteness in the source distribution, the diffusive propagation of protons in magnetic fields (note that the universal spectrum does not depend on the propagation mode as stated by the propagation theorem [30]), and the cosmological evolution with parameters similar to those observed for active galactic nuclei do not spoil the agreement of the dip with the observational data. The strong evolution of the sources leads to a flatter injection spectrum, $\gamma_g \approx 2.4$–2.5, and to fitting the observed spectrum at lower energies [20]. The steep generation spectra with $\gamma_g \approx 2.6$–2.7, source energetics, and models of acceleration with low content of nuclei are also discussed in Refs. [20,22].

The energy calibration of the detectors based upon the position of the dip provides one more clue to the fact that the agreement with observations as illustrated in Fig. 1 is unlikely to be accidental. We perform the calibration in the following way: for each of the three detectors, AGASA, HiRes, and Yakutsk, independently, we allow for a shift of the energy bins inside the dip by a factor λ to reach the minimum χ^2 in the fit. This procedure results in $\lambda_{\rm Ag} = 0.9$, $\lambda_{\rm Hi} = 1.2$, and $\lambda_{\rm Ya} = 0.9$ for the AGASA, HiRes, and Yakutsk detectors, respectively. After this energy shift the absolute fluxes of all detectors in the region of the dip and beyond agree with high precision (see figures in [20,22]).

At $E \geq 1 \times 10^{19}$ eV the dip shows a flattening, which explains the ankle, seen in the data in Fig. 1 at this energy. We remind the reader again about our definition of the ankle as the flat part of the spectrum (in our case the dip) followed from the high-energy side. One can check from Fig. 1 that the beginning of the ankle for e.g. HiRes data gives $E_a \approx 1 \times 10^{19}$ eV.

By definition, the modification factor cannot exceed unity. At energies $E < 1 \times 10^{18}$ eV the modification factors of AGASA-Akeno and HiRes exceed this bound. This signals the appearance of another component, which is most probably given by galactic cosmic rays. This is the first indication in favor of a transition from extragalactic to galactic cosmic rays at $E \sim 1 \times 10^{18}$ eV.

The transition from galactic to extragalactic cosmic rays in the dip scenario is displayed in Fig. 2 (left panel). The

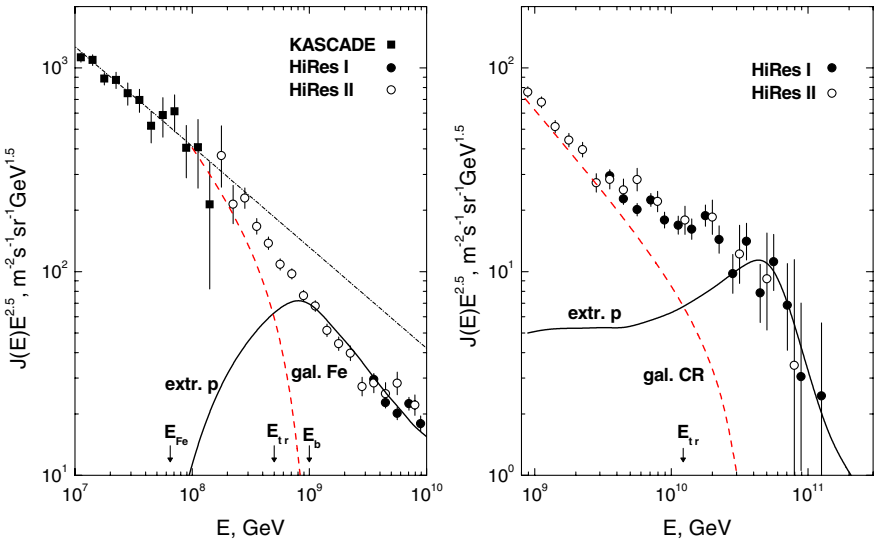

FIG. 2 (color online). Left panel: the second-knee transition. The extragalactic proton spectrum is shown for the $E^{-2.7}$ generation spectrum and for propagation in a magnetic field with $B_c = 1$ nG and $l_c = 1$ Mpc, with the Bohm diffusion at $E \lesssim E_c$. The distance between sources is $d = 50$ Mpc. $E_b = E_{\rm cr} = 1 \times 10^{18}$ eV is the beginning of the transition, $E_{\rm Fe}$ is the position of the iron knee, and $E_{\rm tr}$ is the energy where the galactic and extragalactic fluxes are equal. The dash-dot line shows the power-law extrapolation of the KASCADE spectrum to higher energies, which in fact has no physical meaning, because of the steepening of the galactic spectrum at $E_{\rm Fe}$. Right Panel: the ankle transition, for the injection spectrum of extragalactic protons E^{-2}. In both cases the dashed line is obtained as a result of subtracting the extragalactic spectrum from the observed all-particle spectrum.

steep galactic component intersects the flat extragalactic proton component, which looks rising with energy on the graph because of the multiplication by $E^{2.5}$. This effect is further strengthened because of the diffusive propagation included in the calculations. One can clearly see the appearance of the second knee (very similar to the knees observed by KASCADE) that describes this transition. The dashed line is the inferred galactic cosmic ray spectrum.

The right panel shows the transition in the traditional ankle model.

The anisotropy expected in the dip scenario does not seem to lead to impressive signatures. At 10^{15} eV the observed anisotropy is small and, if the knee is indeed due to a gradually heavier composition at higher energies, the anisotropy expected at the iron knee ($\sim 8 \times 10^{16}$ eV) is the same as that of protons at 3×10^{15} eV, the proton knee. The second knee defines the beginning of the transition to extragalactic cosmic rays. At this energy the composition, in the context of the dip scenario, should suffer a rather sharp change to a proton-dominated one, which has to be complete at 10^{18} eV. Extragalactic protons are most likely isotropic to a large extent: the loss length of protons in the energy range 10^{17}–10^{18} eV is in fact of the same order of magnitude as the cosmological horizon. In the case of straight line propagation this distance is certainly larger than the correlation length which describes the statistical properties of gravity-induced clustering of the large scale structure of the universe. The flux of cosmic rays from a given direction, in this energy range, is an estimate of the mean density of sources along the line of sight, which, however, needs to be very close to the mean density, since the line of sight extends over an appreciable fraction of the universe. We conclude that in this case the flux of protons should be isotropic to a high level.

In the presence of a magnetic field in the intergalactic medium, which may induce diffusive motion in the low-energy region we are interested in, the issue of anisotropy becomes more complex. As discussed in several previous works [31,32], a magnetic field may induce a magnetic horizon: if the closest source is at distance R from the Earth, the propagation time may exceed the age of the universe, in which case the flux at the energies for which this effect is present is exponentially suppressed.

This phenomenon affects the propagation of particles with lower energies, for which the propagation time is the longest. Assuming that particles with energies 10^{17}–10^{18} eV manage to reach the Earth from the closest source, at distance R, the flux of cosmic rays is quasi-isotropic, but not exactly so. In the diffusive regime with the spatial diffusion coefficient $D(E) = \frac{1}{3}\lambda(E)c$, where $\lambda(E)$ is the energy-dependent path length for diffusion, the anisotropy can be written as

$$\delta(E) = \frac{I_{\rm max} - I_{\rm min}}{I_{\rm max} + I_{\rm min}} = \frac{3D(E)}{c} \frac{1}{n(E,r)} \frac{\partial n(E,r)}{\partial r}, \qquad (2)$$

where $I(E)$ is the flux of cosmic rays, $n(E, r)$ is the particle distribution function of cosmic rays at zero order in the anisotropy, namely, the isotropic component, and r is the

distance from the source. For a single source, the number density of particles from the source is $n(r) = \frac{Q(E)}{4\pi r D(E)}$. Therefore

$$\delta = \lambda(E)/R. \tag{3}$$

The path length $\lambda(E)$ can be related to the power spectrum $P(k)$ of the fluctuations of the turbulent magnetic field through

$$\lambda(E) = r_L(E)\frac{B_0^2}{\int_{1/r_L(E)}^{\infty} dk P(k)}, \tag{4}$$

where $P(k)$ is normalized in a way that $\int_{1/L_0}^{\infty} dk P(k) = \eta B_0^2$, with $\eta < 1$ being the fraction of the turbulent field relative to the ordered field B_0. For Bohm diffusion $\lambda(E) = r_L(E)$. For a Kolmogorov spectrum, $P(k) \propto k^{-5/3}$, and one can show that

$$\begin{aligned}\lambda(E) &= r_L(E)^{1/3} L_0^{2/3}(1/\eta) \\ &= (1/\eta)0.1\ \mathrm{Mpc} E_{17}^{1/3} B_{-9}^{-1/3} L_{0,\mathrm{Mpc}}^{2/3},\end{aligned} \tag{5}$$

where B_{-9} is the strength of the ordered magnetic field in units of 10^{-9} Gauss and E_{17} is the cosmic ray energy in units of 10^{17} eV. At energies somewhat larger than 10^{17} eV (for the reference values of the parameters used here) the propagation rapidly loses its diffusive character, unless the magnetic field is unreasonably large (even for $\eta \sim 1$). From Eq. (5) one can also see that, in order to obtain that particles with energy $\sim 10^{18}$ eV suffer the effect of a propagation time longer than the age of the universe, the local magnetic field must be in the range of a few 10^{-8} Gauss. For a single source at distance 50 Mpc, the anisotropy could be of order $\sim 10^{-3}$ for energies $\sim 10^{18}$ eV. For the case of Bohm diffusion the anisotropy is easily calculated as $\delta = r_L/R$. For a source at 50 Mpc distance one obtains $\delta = 2 \times 10^{-3} E_{17} B_{-9}^{-1}$. The numerical value of the expected anisotropy is, not surprisingly, close to that for Kolmogorov spectrum, since in the energy region of interest the power spectrum was assumed to reach saturation (namely, the Larmor radius is roughly equal to the size of the largest eddy).

These predictions rely, however, on several assumptions, none of which appears to be particularly justified. For instance, the density of sources could be large enough, such that the anisotropy from a single source is compensated by a spatial distribution of sources. Moreover, even if the flux reaching the Galaxy is slightly anisotropic, the effect of the galactic magnetic field is likely to reduce such anisotropy, possibly to undetectable levels.

III. THE ELONGATION RATE

As discussed in the previous section, in the dip scenario the transition from galactic to extragalactic cosmic rays occurs sharply enough, changing from galactic iron to extragalactic protons (see left panel of Fig. 2). This must result in a steep dependence of the depth of shower maximum $X_{\max}$ (actually its mean value) as a function of energy in the range between 10^{17} and 10^{18} eV. Below 3×10^{17} eV we expect $X_{\max}$ being dominated by galactic iron nuclei. Above 10^{18} eV the proton-dominated extragalactic flux determines the average $X_{\max}$ observed. In this section we calculate the elongation rates for the dip and ankle models and compare them with observations.

The results of our benchmark calculations for proton-induced and iron-induced showers are shown in Fig. 3 (left panel): we used a standard extensive air shower (EAS) simulation code, CONEX [33], in order to employ different hadronic interaction models (here and in the following we simulated 5000 and 1000 showers per energy for p- and Fe-induced EAS, correspondingly). The solid lines in the figure refer to QGSJET [34], the dashed ones to QGSJET-II [35] (version 03), and the dotted lines to SIBYLL 2.1 [36]. The results of the three model calculations are within ~ 20 g cm^{-2} from each other and the predicted $X_{\max}$ values for proton- and iron-induced EAS are separated at basically all energies by ~ 100 g cm^{-2}. As discussed in the

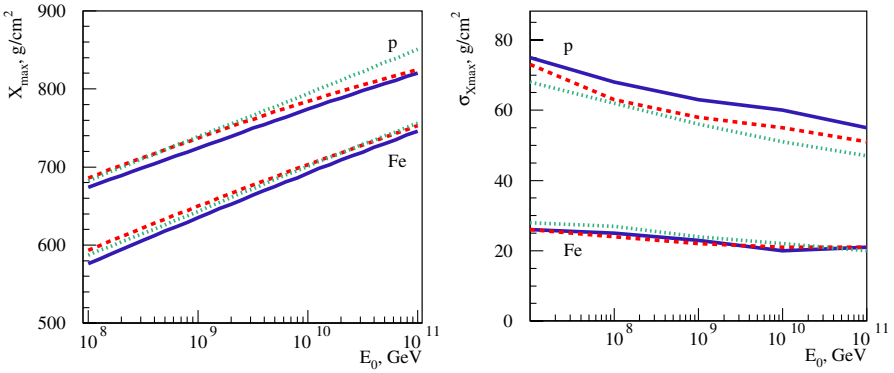

FIG. 3 (color online). Average penetration depth $\bar{X}_{\max}$ (left panel) and the variance of $X_{\max}$ distribution $\sigma_{X_{\max}}$ (right panel) as functions of energy for protons (upper curves) and iron nuclei (lower curves) as calculated using QGSJET, QGSJET-II, and SIBYLL models—solid, dashed, and dotted lines, correspondingly.

next section, the predicted shower maximum is described by a distribution whose width varies with energy [see Fig. 3 (right panel)]. In the low-energy part, around 10^{17} eV, the width of the distribution is ~ 25 g cm^{-2} for iron nuclei and ~ 70 g cm^{-2} for proton-initiated showers. These numbers provide a qualitative explanation of the difficulties in discriminating iron showers from proton-induced ones (and even more so for elements of intermediate masses).

Weighing $X_{\mathrm{max},p}(E)$ and $X_{\mathrm{max,Fe}}(E)$ from Fig. 3 (left panel) with the flux of cosmic rays in the form of different chemical components leads to the expected elongation rate:

$$X_{\mathrm{max}}(E) = \frac{J_p(E)\bar{X}_{\mathrm{max},p}(E) + J_{\mathrm{Fe}}(E)\bar{X}_{\mathrm{max,Fe}}(E)}{J_p(E) + J_{\mathrm{Fe}}(E)}. \quad (6)$$

Here J_p and J_{Fe} are the fluxes of protons and iron nuclei expected at energy E in a given model. These fluxes take into account both the galactic contribution and the extragalactic one. In Eq. (6) the quantities $\bar{X}_{\mathrm{max},p}(E)$ and $\bar{X}_{\mathrm{max,Fe}}(E)$ are those shown in Fig. 3 (left panel).

In Fig. 4 we plot the results of our calculations for the penetration depth as a function of energy for the dip scenario (left panel) and for the ankle scenario (right panel) in comparison to experimental data of Fly's Eye [37], HiRes-Mia [38], and HiRes [39].

In the dip scenario (left panel) we identify as a distinctive feature the sharp rise of the penetration depth at energies between 10^{17} eV and 10^{18} eV, reflecting the sharp transition from galactic iron to extragalactic proton-dominated flux. In the calculations presented here we used Bohm diffusion at energies below 1×10^{18} eV. The shape of $X_{\mathrm{max}}(E)$ in the range of energies considered here remains the same for Kolmogorov diffusion, but it becomes smoother for rectilinear propagation of protons or for very small distances between the sources. The transition is completed at $\sim 1 \times 10^{18}$ eV with a composition being strongly dominated by protons. In this calculation we neglect the possibility of a small admixture of nuclei in the extragalactic flux as allowed by the dip model. In the case of 10%–20% admixture of He, the presented elongation curves change only slightly. Taking into account a typical systematic uncertainty in the determination of X_{max} as 20–25 g/cm^2 [38], the data plotted in the left panel agree reasonably well with the dip prediction, especially in the case of the QGSJET model, and the steep rise of the elongation rate at 1×10^{17}–1×10^{18} eV does not contradict the experimental data. In the case of the ankle model, the transition is much smoother in terms of the chemical composition (right panel), the latter becoming proton dominated only at energies above 10^{19} eV. In the energy range $(1\text{–}5) \times 10^{19}$ eV the disagreement with the data exceeds the systematic error in X_{max}.

The comparison with the recent Auger data [40] is illustrated separately in Fig. 5. For the dip model (left panel) the disagreement does not exceed 23 g cm^{-2}, if we exclude the highest energy data point.

For the ankle model this disagreement reaches ~ 60 g/cm^2 in the energy range $(5\text{–}20) \times 10^{17}$ eV. In principle, in models which assume a rigidity-dependent galactic CR acceleration or propagation, one may expect some admixture of silicon or even lighter nuclei around 10^{17} eV (see, e.g., [41]), which rapidly disappear at higher energies. Depending on the relative abundance of such lighter elements, the predicted X_{max} in the left panels of Figs. 4 and 5 may be slightly shifted upwards in the lowest energy bins, while the corresponding energy dependence in the interval 10^{17}–2×10^{17} may flatten—as the importance of extragalactic protons is then partly compensated by the disappearance of galactic nuclei which are lighter than iron. An analysis of such effects goes beyond the scope of the present paper.

The case of a mixed composition has been discussed in [24,25], and it is intermediate between the two cases of the

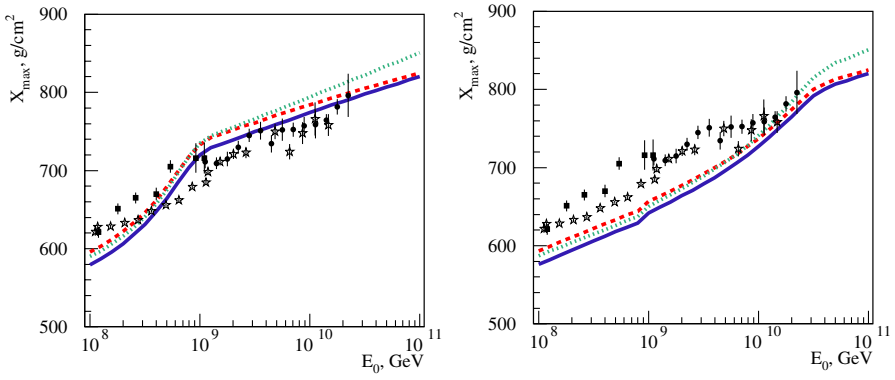

FIG. 4 (color online). Left panel: elongation rate for the dip scenario. Right panel: elongation rate for the ankle scenario. The three lines, which present the calculations, are labeled as in Fig. 3: solid, dashed, and dotted lines correspond to QGSJET, QGSJET-II, and SIBYLL models, respectively. The data points are the measurements of Fly's Eye (stars) [37], HiRes-Mia (squares) [38], and HiRes (circles) [39] experiments.

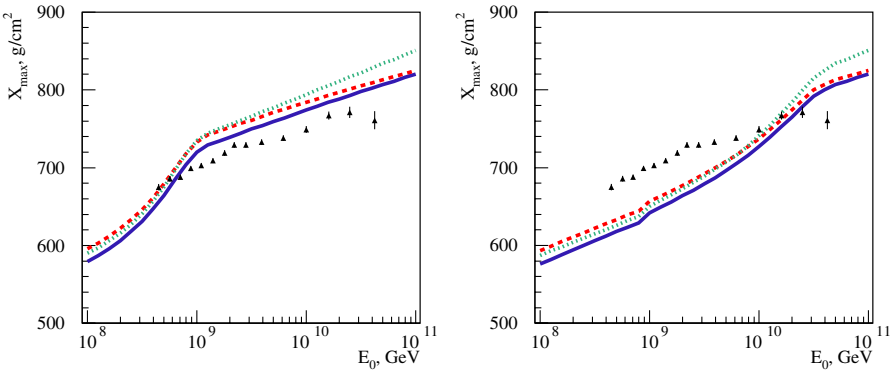

FIG. 5 (color online). Elongation rates for the dip scenario (right panel) and for that of the ankle (left panel) in comparison with the Auger data [40]. The three lines are labeled as in Fig. 3.

dip and the ankle models. The agreement of the calculated elongation rate with the data is the best among these three models, and the choice of a chemical composition at the source always allows one to obtain a good fit to the observations. As far as Auger data are concerned, the mixed-composition model agrees with the break in elongation rate at 2×10^{18} eV and contradicts the highest energy point in Auger measurements. The authors claim as the main feature of the model the appearance of a plateau in the elongation rate, to be searched for in future, more precise data.

IV. THE $X_{\max}$ DISTRIBUTION

We want to emphasize here that a more effective tool to assess the chemical composition in the transition region is provided by an analysis of the distribution of the shower maximum, which is more sensitive to the primary composition than the elongation rates plotted in Fig. 4. Our benchmark calculation for the distribution of $X_{\max}$ yields the widths shown in Fig. 3 (right panel), as a function of the total energy of the nucleus. The results refer to protons (upper curves) and to iron nuclei (lower curves) for the same interaction models as discussed in the previous section. It is easy to see that the model dependence of the calculated $\sigma_{X_{\max}}$ is much weaker than for the average position of the shower maximum. For proton-induced EAS the difference in the distribution width is mainly due to different total inelastic $\sigma^{\text{inel}}_{p\text{-air}}$ and diffractive $\sigma^{\text{diffr}}_{p\text{-air}}$ proton-air cross sections predicted by models [42]. It is noteworthy that the present model differences for $\sigma^{\text{inel}}_{p\text{-air}}$ of 10%–15% will be significantly reduced in the near future, due to the expected precise measurements of the total proton-proton cross section at the CERN Large Hadron Collider. In the case of primary nuclei, the width of the $X_{\max}$ distribution is mainly defined by fluctuations of the number of interacting projectile nucleons in individual nucleus-air collisions [43,44], which are governed by the geometry of the interaction (primarily by the variations of the impact parameter of the collision) and are practically model independent. Additional model dependence may come from the treatment of the fragmentation of the nuclear spectator part. However, while the two extreme scenarios—conservation of the spectator part as a single nuclear fragment or its total breakup into independent nucleons—give rise to rather different predictions for EAS fluctuations [44], realistic fragmentation models, being tuned to the relevant accelerator data, produce very similar results for $\sigma^{A\text{-air}}_{X_{\max}}$, as is illustrated by Fig. 3 (right panel).

The power of using the distribution of penetration depths at given energy of the primary particle is illustrated in Fig. 6, where we show our results (lines labeled as in the previous section) compared to the data of the Fly's Eye Collaboration [45]. The different panels refer to different energy bins. The left (right) panel presents the results for the dip (ankle) scenario. To account for the reported experimental resolution of the shower maximum of 45 g cm^2, we introduced the corresponding smearing of the calculated $X_{\max}$ values, using a Gaussian distribution.

In the lowest energy bin [(1–3) $\times 10^{17}$ eV], the shape of the distribution is well described by the dip model, while the fit of the ankle model seems rather poor. It is in fact interesting to notice that the tail at depths larger than $\sim$700 g cm^{-2} can be properly fit only if there is an appreciable amount of a light component. This is the role played by the small fraction of protons in the top left panel of Fig. 6. Moving downwards in Fig. 6 corresponds to moving towards larger energies, and the peak of the distributions (for both models) shifts to larger penetration depths, also due to a lighter mean composition in both cases.

In the energy bin (3–10) $\times 10^{17}$ eV, the fit provided by the dip model still seems acceptable and is definitely better than for the ankle model. However, there seems to be a slight excess of the light component which manifests itself in the tail of the distribution. This could suggest that a component slightly heavier than protons should be present. This seems to be confirmed by the plots referring to higher

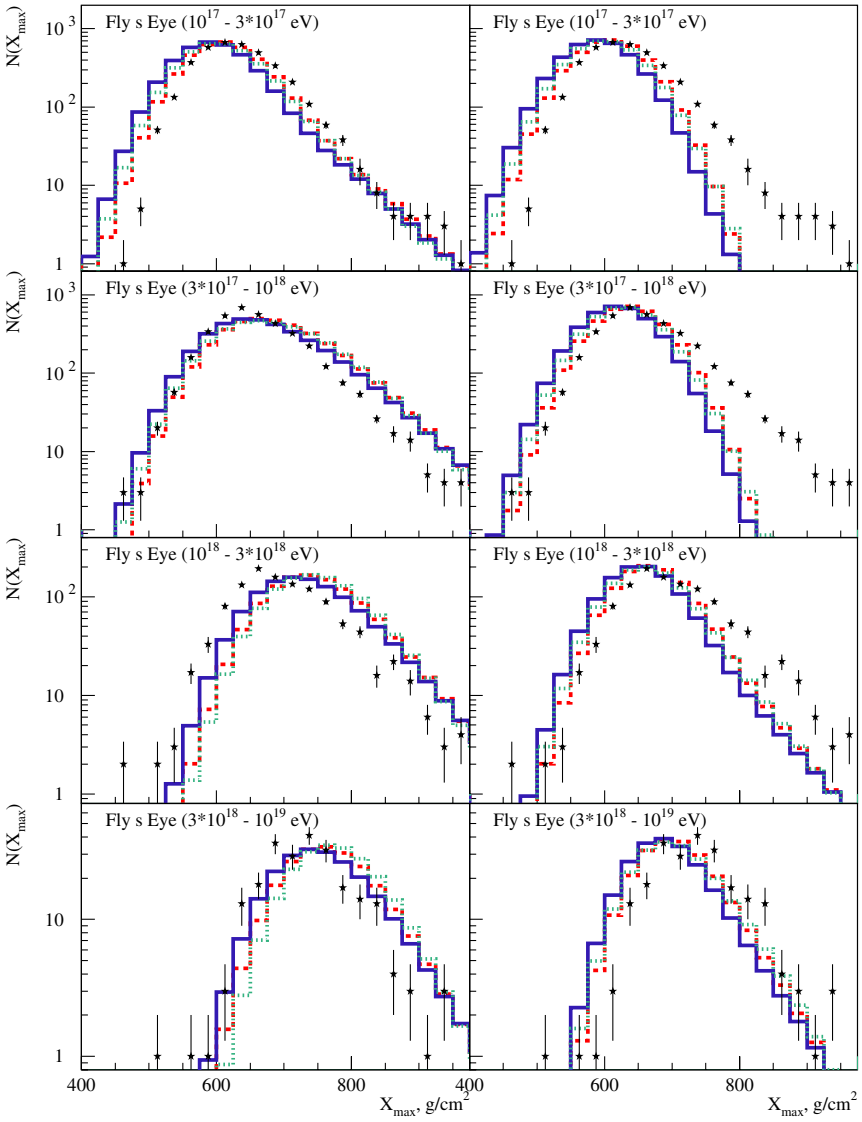

FIG. 6 (color online). Predicted $X_{\max}$ distribution for the dip scenario (left panels) and for the ankle scenario (right panels) in different energy bins in comparison with Fly's Eye data [45] (points).

energies. On the other hand, this effect is more apparent in the energy bin (3–10) $\times$ 10^{17} eV, namely, where the transition actually happens in the dip scenario. The exact shape and mix of the different components in this energy region (galactic plus extragalactic) is, however, dependent upon some details, such as the presence of an extragalactic magnetic field, the possibility of a solar-wind-like modulation effect due to a galactic wind, which we have currently no deep insight into.

In Fig. 7 we show a similar comparison to the data of the HiRes Collaboration. The left (right) column refers to the dip (ankle) model. In the lowest energy bin [(3–6) $\times$ 10^{17} eV] we compared our results with HiRes-Mia data [38]. In the middle bin ($E_0 \simeq 10^{18}$ eV) we used HiRes mono data [46]. In the highest energy bin ($E_0 > 10^{18}$ eV) the comparison was made with HiRes stereo data [47]. Again, a Gaussian smearing of the calculated $X_{\max}$ values has been introduced according to the reported experimental resolutions of 45, 41, and 30 g cm^{-2}, respectively.

The dip scenario fits the data at all energies very nicely, while it is safe to claim that the ankle scenario does not describe them correctly. In the energy bin centered at 10^{18} eV the peak of the distribution is already placed at the location expected for proton showers, as expected for the dip scenario and as already suggested by the plots on the elongation rate shown in the previous section. In the highest energy bin, the composition appears to be stabilized to a proton-dominated one. These conclusions are rather independent of the interaction model adopted for the calculations.

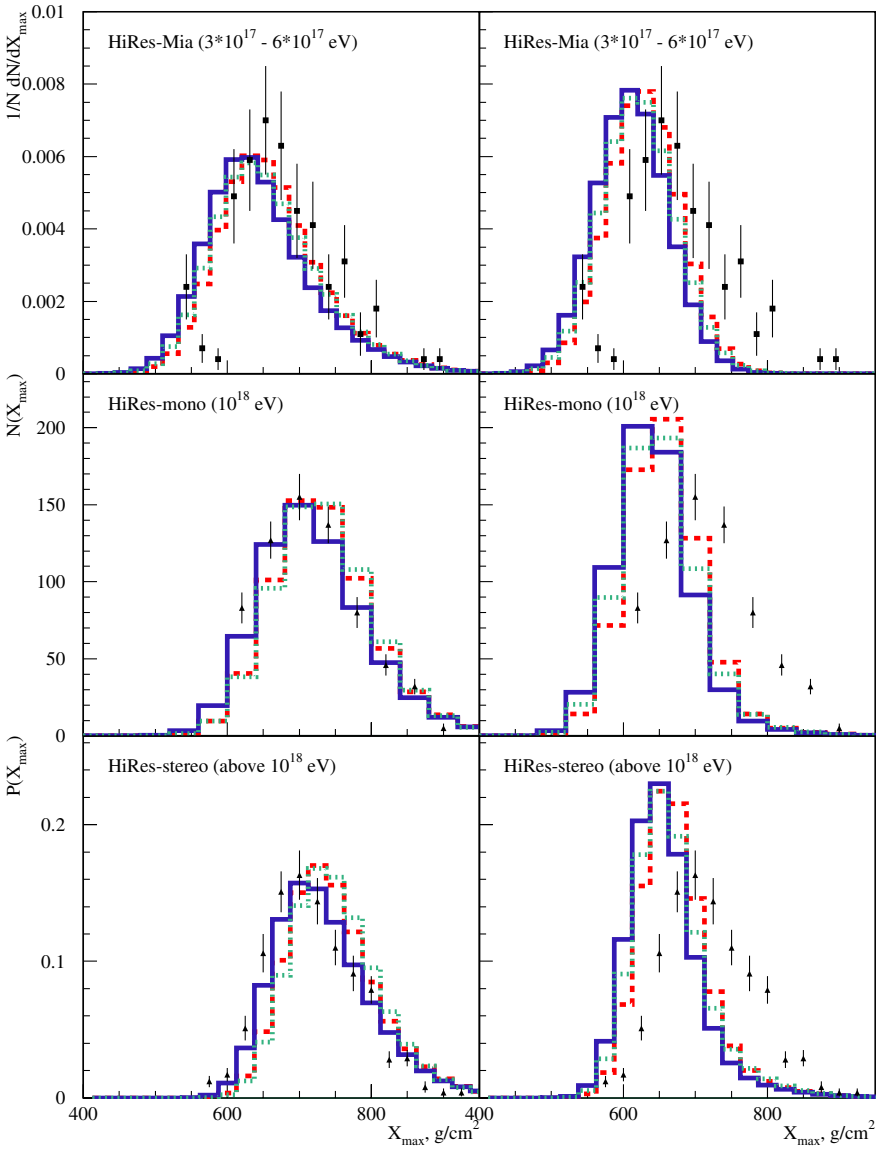

FIG. 7 (color online). Predicted $X_{\max}$ distribution for the dip scenario (left panels) and for the ankle scenario (right panels) in different energy bins in comparison with HiRes data (points).

V. DISCUSSION AND CONCLUSIONS

We discussed the signatures of the transition from galactic to extragalactic cosmic rays, in terms of spectrum, anisotropy, and chemical composition. Special emphasis has been given to the measurement of the elongation rate and to the width of the distribution of penetration depths $X_{\max}$ in given energy bins.

The implications of the different models of the transition for the *spectrum* are profound and, in principle, the easiest to measure: in the ankle scenario the transition occurs at relatively high energy, $\sim 10^{19}$ eV, as a result of the intersection of a steep power-law galactic component and a flatter extragalactic spectrum. The ankle scenario is not compatible with the basic version of the standard model for galactic cosmic rays, since it requires a galactic (iron-dominated) component which extends above $\sim 10^{19}$ eV.

The dip in the data, as observed by all experiments operating in the relevant energy region, is naturally explained as being the pair-production dip. In this case, cosmic rays in the energy region 10^{18}–10^{19} eV are mainly extragalactic protons (with possibly 10%–15% contamination of nuclei), and the transition between galactic and extragalactic cosmic rays results in a faint feature in the all-particle spectrum, known as the second knee. It represents the lower part of the transition region and occurs, in the dip scenario, because of the intersection of a steep galactic spectrum with a flatter extragalactic one.

In the dip model, the flattening in the spectrum of the extragalactic component is present both in the case of quasirectilinear and for diffusive propagation. In the latter case the effect may be more evident, thereby reflecting a flux suppression due to the anti-Greisen-Zatsepin-Kuzmin effect and a magnetic horizon [22,31,32] if the magnetic field in the intergalactic medium is not too small (of order of 0.1–1 nG). The effect is stronger in the case of Bohm diffusion as compared with Kolmogorov diffusion.

The dip scenario is fully consistent with the SNR paradigm for the origin of galactic cosmic rays, according to which galactic iron nuclei should be accelerated at most up to $\sim 10^{17}$ eV.

The pair-production dip fits impressively well the observational data. When the energy bins of each experiment are shifted to achieve the minimum χ^2 in comparison with the calculated position of the dip (this is what we refer to as the energy calibration of a detector), the absolute fluxes measured by all experiments agree well with each other. This agreement gives another evidence that the spectral coincidence of the pair-production dip with the data is unlikely to be accidental.

Despite this impressive result, one can fit the data also with a weighted superposition of different chemical elements at the source, injected with relatively flat spectra ($\sim E^{-2.3}$). In this mixed-composition scenario, the transition is completed at $\sim 3 \times 10^{18}$ eV, thereby being marginally consistent with the basic predictions of the standard model for the origin of galactic cosmic rays, based on the SNR paradigm.

Our predictions on the *anisotropy* signal are not exciting: for the dip model, in both cases of rectilinear (low magnetic field) and diffusive propagation (larger field) the expected anisotropy is low and most likely undetectable, especially when the isotropizing effect of the galactic magnetic field is taken into account. These conclusions hold also in the mixed-composition model. In the ankle scenario, there might be a residual disc anisotropy associated with the highest energy iron nuclei of galactic origin.

The most effective tool to infer the nature and location of the transition is an accurate (and difficult) measurement of the *chemical composition* in the energy region between 10^{17} and 10^{19} eV. Here we discussed the elongation rate and the $X_{\max}$ distribution as two possible tools to gather this information. We also compared the predictions for the dip and ankle scenarios with available data of the Fly's Eye, HiRes, and Pierre Auger collaborations. The case of a mixed composition has been investigated in detail in [26] in terms of the elongation rate and was therefore not addressed further here.

Our benchmark calculations for the penetration depth for proton- and iron-induced showers have been carried out with SIBYLL, QGSJET, and QGSJET-II hadronic interaction models. The same interaction codes have been used throughout all other calculations we carried out. The intrinsic uncertainty in the mean value of the penetration depth as due to uncertainties in the interaction models is ~ 20 g cm^{-2}, while the average separation between proton- and iron-initiated showers as a function of energy remains of ~ 100 g cm^{-2}. The distribution of values of $X_{\max}$ around the mean has a typical width of 70 g cm^{-2} for protons and 25 g cm^{-2} for iron. This makes it immediately clear why it is particularly hard to nail down the composition at given energy: only a very large number of showers can lead to an unambiguous tagging of the composition in terms of the elongation rate. The task becomes even harder if elements with intermediate masses between hydrogen and iron are present in appreciable quantities.

We calculated the elongation rate expected for the dip and ankle scenarios. The ankle model provides a bad fit to all sets of data. The dip scenario is qualitatively much better, but it still provides only a rough fit to all data sets in agreement only within systematic energy errors. An exceptional case is given by the HiRes data which closely follow the behavior predicted by the dip model of the transition. This is also consistent with the original HiRes claim that the composition becomes proton-dominated already at 10^{18} eV. The general trend observed is that of a transition from a heavy-dominated composition to a light one in the energy range between 10^{17} eV and a few times 10^{18} eV.

The most peculiar prediction of the dip model is that there should be a sharp transition from heavy to light dominance, starting at the second knee and ending at 10^{18} eV with a proton-dominated composition. We calculated the elongation rate for this transition using the most physically justified scenario of diffusive propagation. In the case of rectilinear propagation the elongation rate becomes smoother.

The mixed-composition scenario leads to a shallower transition which is completed only at $E \simeq 3 \times 10^{18}$ eV. This model seems to provide a better fit to the available data on the elongation rate (with the possible exception of the HiRes-Mia results), though the latter show a wide spread which reflects the inherent experimental systematics.

We also analyzed the predictions of the dip and ankle models in terms of the distribution of $X_{\max}$, which is essentially determined by the corresponding intrinsic width for a particular type (mass number) of the primary particle, convoluted with the superposition of the heavy and light components, as provided by the galactic and extragalactic contributions, respectively. The calculations have been carried out in energy bins suitable for the comparison with available data of the Fly's Eye and HiRes collaborations.

The lowest energy bin in the Fly's Eye data [$(1–3) \times 10^{17}$ eV] is very interesting: the comparison of the expected distributions for the dip and ankle scenarios shows that, while the peak of the distribution in the two cases is essentially at the same position, ~ 600 g cm^{-2}, as expected

for iron-dominated showers, the tail of the distribution cannot be explained unless a substantial amount of protons is present, as expected in the dip model. This part of the distribution cannot be fit by the ankle scenario. The dip model also provides a good fit to the Fly's Eye data in the higher energy bins. The ankle and dip models provide basically the same distribution of $X_{\max}$ only at energies in excess of 10^{19} eV, where the composition becomes proton dominated in both scenarios.

It is interesting to notice that, in the two Fly's Eye data bins that contain the transition, as expected in the dip scenario [$(3–10) \times 10^{17}$ eV and $(1–3) \times 10^{18}$ eV], the predicted distributions show a slight excess of the light component in the tail. This might suggest that a somewhat heavier component might be needed to improve the fit.

The comparison with HiRes data on the distribution of $X_{\max}$ in the three energy bins $(3–6) \times 10^{17}$ eV (from HiRes-Mia), $E_0 \simeq 10^{18}$ eV (from HiRes mono), and $E_0 > 10^{18}$ eV (from HiRes stereo) shows a complete agreement with the dip model. The ankle model, once more, provides a bad fit to the data.

All these conclusions are very weakly dependent upon the model for interactions in the atmosphere.

ACKNOWLEDGMENTS

The work of R. A., V. B., and P. B. has been partially supported by ASI under Contract No. ASI-INAF I/088/06/0 for theoretical studies in High Energy Astrophysics. The work of P. B. was also partially funded through PRIN 2006.

[1] D. R. Bergman and J. W. Beltz, J. Phys. G **34**, R359 (2007).
[2] E. G. Berezhko, Proceedings of ICRC (Hamburg), Rapporteur and Highlight papers, 2001, p. 226.
[3] P. Blasi, E. Amato, and D. Caprioli, Mon. Not. R. Astron. Soc. **375**, 1471 (2007).
[4] J. S. Warren *et al.*, Astrophys. J. **634**, 376 (2005).
[5] A. R. Bell, Mon. Not. R. Astron. Soc. **353**, 550 (2004).
[6] E. Amato and P. Blasi, Mon. Not. R. Astron. Soc. **364**, 76 (2005).
[7] E. Amato and P. Blasi, Mon. Not. R. Astron. Soc. **371**, 1251 (2006).
[8] V. S. Ptuskin and V. N. Zirakashvilli, Astron. Astrophys. **429**, 755 (2005).
[9] E. G. Berezhko and H. J. Völk, arXiv:0704.1715.
[10] P. O. Lagage and C. J. Cesarsky, Astron. Astrophys. **118**, 223 (1983); **125**, 249 (1983).
[11] T. Antoni *et al.* (KASCADE Collaboration), Astropart. Phys. **24**, 1 (2005).
[12] M. Aglietta *et al.* (EAS-TOP Collaboration), Proceedings of the 28th International Cosmic Ray Conference, Tsukuba, Japan, 2003, p. 183.
[13] T. Antoni *et al.* (KASCADE Collaboration), Astrophys. J. **604**, 687 (2004).
[14] D. De Marco, P. Blasi, and T. Stanev, arXiv:0705.3184 [J. Cosmol. Astropart. Phys. (to be published)].
[15] A. M. Hillas, arXiv:astro-ph/0607109; J. Phys. G **31**, R95 (2005); Nucl. Phys. B, Proc. Suppl. **136**, 139 (2004); E. Waxmam, Phys. Rev. Lett. **75**, 386 (1995); M. Vietri, Astrophys. J. **453**, 883 (1995); T. Wibig and A. W. Wolfendale, J. Phys. G **31**, 255 (2005).
[16] M. Lemoine and B. Revenu, Mon. Not. R. Astron. Soc. **366**, 635 (2006).
[17] C. T. Hill and D. N. Schramm, Phys. Rev. D **31**, 564 (1985).
[18] S. Yoshida and M. Teshima, Prog. Theor. Phys. **89**, 833 (1993).
[19] V. S. Berezinsky and S. I. Grigorieva, Astron. Astrophys. **199**, 1 (1988).
[20] V. Berezinsky, A. Z. Gazizov, and S. I. Grigorieva, Phys. Rev. D **74**, 043005 (2006).
[21] V. Berezinsky, A. Z. Gazizov, and S. I. Grigorieva, Phys. Lett. B **612**, 147 (2005).
[22] R. Aloisio, V. Berezinsky, P. Blasi, A. Gazizov, S. Grigorieva, and B. Hnatyk, Astropart. Phys. **27**, 76 (2007).
[23] M. Kachelriess and D. Semikoz, Phys. Lett. B **634**, 143 (2006).
[24] D. Allard *et al.*, Astron. Astrophys. **443**, L29 (2005).
[25] D. Allard *et al.*, Astron. Astrophys. **443**, L29 (2005).
[26] D. Allard, A. V. Olinto, and E. Parizot, arXiv:astro-ph/0703633.
[27] V. Berezinsky, S. Grigorieva, and B. Hnatyk, Astropart. Phys. **21**, 617 (2004).
[28] T. Stanev *et al.*, Phys. Rev. D **62**, 093005 (2000).
[29] V. Berezinsky, A. Gazizov, and S. Grigorieva, arXiv:0706.2643.
[30] R. Aloisio and V. Berezinsky, Astrophys. J. **612**, 900 (2004).
[31] M. Lemoine, Phys. Rev. D **71**, 083007 (2005).
[32] R. Aloisio and V. Berezinsky, Astrophys. J. **625**, 249 (2005).
[33] T. Bergmann *et al.*, Astropart. Phys. **26**, 420 (2007); T. Pierog *et al.*, Nucl. Phys. B, Proc. Suppl. **151**, 159 (2006).
[34] N. N. Kalmykov, S. S. Ostapchenko, and A. I. Pavlov, Bulletin of the Russian Academy of Sciences Physics **58**, 1966 (1994); Nucl. Phys. B, Proc. Suppl. **52**, 17 (1997).
[35] S. Ostapchenko, Phys. Rev. D **74**, 014026 (2006); Nucl. Phys. B, Proc. Suppl. **151**, 143 (2006).
[36] R. S. Fletcher, T. K. Gaisser, P. Lipari, and T. Stanev, Phys. Rev. D **50**, 5710 (1994); R. Engel *et al.*, Proceedings of the 26th International Cosmic Ray Conference, Salt Lake City, USA, 1999, p. 415.
[37] D. J. Bird *et al.* (Fly's Eye Collaboration), Phys. Rev. Lett. **71**, 3401 (1993).
[38] T. Abu-Zayyad *et al.* (HiRes-Mia Collaboration), Astrophys. J. **557**, 686 (2001); P. Sokolsky, Proceedings

of the 30th International Cosmic Ray Conference, Merida, 2007.
[39] R. U. Abbasi *et al.* (HiRes Collaboration), Astrophys. J. **622**, 910 (2005).
[40] M. Unger *et al.* (Pierre Auger Collaboration), arXiv:0706.1495.
[41] A. M. Hillas, J. Phys. Conf. Ser. **47**, 168 (2006).
[42] K. Belov *et al.* (HiRes Collaboration), Czech. J. Phys. **A56**, A313 (2006).
[43] J. Engel, T. K. Gaisser, T. Stanev, and P. Lipari, Phys. Rev. D **46**, 5013 (1992).
[44] N. N. Kalmykov and S. S. Ostapchenko, Phys. At. Nucl. **56**, 346 (1993).
[45] D. J. Bird *et al.* (Fly's Eye Collaboration), Proceedings of the 23rd International Cosmic Ray Conference, Calgary, Canada, 1993, p. 38.
[46] D. R. Bergman *et al.* (HiRes Collaboration), Nucl. Phys. B, Proc. Suppl. **136**, 40 (2004).
[47] P. Sokolsky *et al.* (HiRes Collaboration), Proceedings of the 29th International Cosmic Ray Conference, Pune, India, 2005, p. 381.
[48] K. Shinozaki and M. Teshima, Nucl. Phys. B, Proc. Suppl. **136**, 18 (2004).
[49] R. U. Abbasi *et al.* (HiRes Collaboration), Phys. Rev. Lett. **92**, 151101 (2004).
[50] A. V. Glushkov *et al.* (Yakutsk Collaboration), Proceedings of the 28th International Cosmic Ray Conference, Tsukuba, Japan, 2003, p. 389.
[51] L. Perrone *et al.* (Pierre Auger Collaboration), arXiv:0706.2643.